Deep Burn Modular High Temperature Reactors

Project Summary Report
For period
November 1, 2006 to October 31, 2007

Submitted to
General Atomics
La-Jolla, California

UCBTH-07-007

By
E. Greenspan, P.F. Peterson, M. Fratoni and A. Cisneros
University of California
Department of Nuclear Engineering
Berkeley, CA 94720

October 31, 2007

Acknowledgment

This report is based upon work supported by the General Atomics company under Award No. 4500002492

Table of Contents

1. Introduction

General Atomics (GA) asked the Department of Nuclear Engineering of the University of California at Berkeley (UCB) to perform an independent evaluation of the capability of their Modular Helium cooled Reactor (MHR) design to transmute transuranium isotopes (TRU) extracted from the fuel discharged from Light Water Reactors (LWR), and to search for improvement possibilities. The specific design we were to evaluate is also referred to as the "Deep Burn" MHR or DB-MHR. Following are specific objectives defined for this project:

1. Benchmark our upgraded MOCUP code system and cross-section libraries against the Reactor Physics Benchmark Specification for the DB-MHR Actinide Burner (R.A. Rucker, General Atomics, May 2002).

2. Apply our verified computational tool to perform an independent verification of the discharge burn-up attainable from a DB-MHR. The core model to be used will account for the double-heterogeneity of the MHR prismatic fuel. Core design, materials properties, temperature distribution, initial TRU composition, design constraints and in-core fuel management scheme will be defined by GA. In addition to the discharge burn-up, determine the discharged fuel characteristics. These characteristics include the isotopic composition, decay heat, spontaneous neutron emission rate and radiotoxicity.

3. Refine the analysis to be done in Task 2 by accounting for axial fuel shuffling and realistic temperature distribution. In addition to the attainable discharge burn-up and discharged fuel characteristics defined above, calculate the reactivity coefficients associated with fuel and graphite temperature change and expansion, the cold zero power-to-hot full power reactivity deficiency and reactivity control requirements.

4. Investigate possibilities for increasing the discharge burn-up of the DB-MHR while maintaining reasonable cycle duration by optimizing the core design and in-core fuel management. Design variables to be considered include the fuel kernel dimensions, TRU-to-C atom ratio and fuel shuffling schemes. Determine the discharged fuel characteristics of the optimal design.

5. Investigate the sensitivity of the attainable discharge burn-up and cycle length to the fed fuel composition. Among the fed fuel types to be examined are TRU from PWR that was discharged at low (33 GWD/t) and high (60 GWD/t) burn-up and that underwent short (5 years) and long (30 years) cooling, as well as weapons grade plutonium. Also establish the sensitivity of the discharged fuel characteristics to the fuel feed composition. Determine the implications of removing the Cm from the discharged fuel.

6. Determine the effect of burnable poisons on achievable burn-up, discharge fuel composition and reactivity coefficients. The burnable poisons are needed to compensate for the beginning-of-cycle excess reactivity and may help in flattening of the core power density. Identify the preferred burnable poison and its distribution in the core.

7. Provide a summary report

Due to issues with a no-cost extension, we were not able to complete Task 6.

The project also preformed comparisons of the performance of He-cooled prismatic core design against alternative reactor designs that were being studied under separate projects, liquid-salt (flibe) cooled pebble-bed core designs (PB-AHTR) and a hydride fueled PWR. These comparisons are also presented in this report.

Towards the termination of this project GA and DOE established a national consortium aimed at performing a similar evaluation but at a much expanded scope and depth. As a result, the UCB effort was redirected to fit within the national consortium evaluation. Following is a summary of the work done at UCB under the original contract with GA.

2. MCNP Model for the Deep Burn Modular Helium-Cooled Reactor

This section summarizes the MCNP model created for the Deep Burn-Modular Helium-cooled Reactor (DB-MHR) study. The model aims to reproduce the full core with all the relevant components in full detail. The first paragraph discusses core geometry and dimensions; the second materials and temperatures; the third the depletion scheme. Unless specified otherwise, all the data were obtained from the file "MHR block design PUMA core specifications" provided by Dr. Francesco Venneri of General Atomic.

2.1 Geometry

The DB-MHR core is composed of 1440 hexagonal blocks arranged in 144 columns, with 10 axially stacked elements per column, forming an annular core (

Figure 1). These graphite blocks are pitched with 108 channels through which the coolant flows and 216 blind channels, the burnable poison.

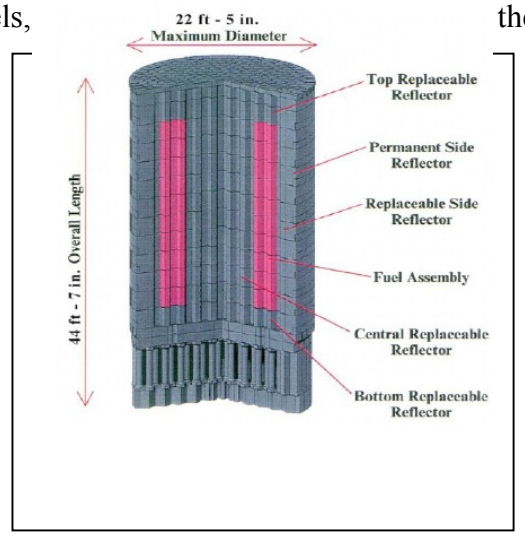

Figure 1 DB-MHR core inner view

A central hole allows accommodating a fuel pick up probe for element handling. The coolant channel diameter is 1.5875 cm but for the 6 channels around the fuel handling hole, whose diameter is only 1.27 cm like the fuel channels. The holes pitch is ~1.88 cm. The fuel is in the form of TRISO coated particles dispersed in a graphite matrix to form

cylindrical fuel compacts (diameter 1.245 cm, length 4.928 cm). Each fuel hole holds 15 compacts. Four dowels are excavated at the top and the bottom of the blocks. Each one houses a pin that connects the blocks one to the other and aligns the coolant channels. The fuel holes under the dowels are only 75.26 cm long and houses 14 compacts instead of 15. The dowels are 4.445 cm in diameter and 1.448 cm deep. All fuel holes are closed at the top by cemented graphite plugs. The burnable poisons holes are located at the corners of the hexagonal block.

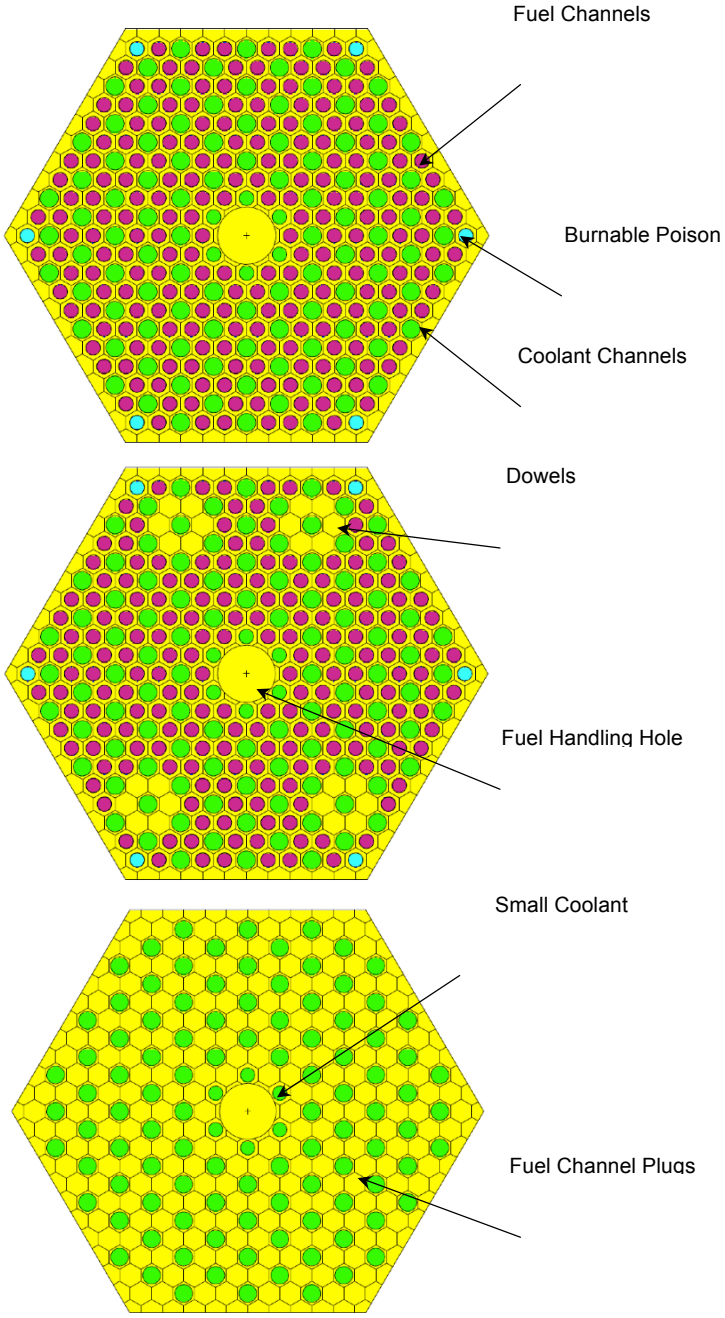

Figure 2 Fuel element horizontal cross section

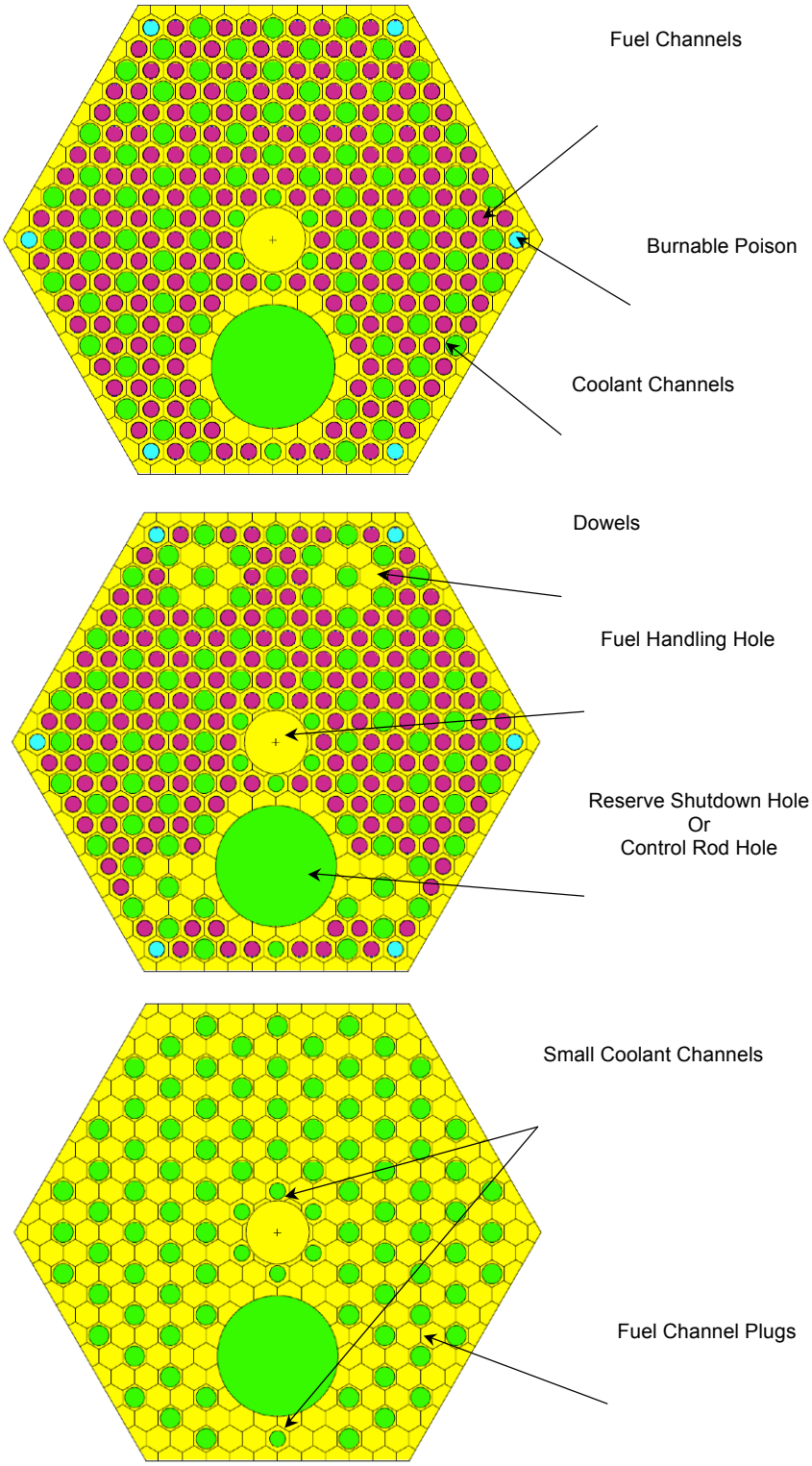

Figure 3 RSC or control rods fuel block horizontal cross section

The DB-MHR core is composed of three different types of fuel elements: (1) the standard fuel element as described above; (2) the reserve shutdown control (RSC) elements that have only 186 fuel holes and 95 coolant channels (7 of which small) so as to accommodate a 9.525 cm diameter hole along the block for control rods insertion; (3) control rods elements that look alike RSC elements but with a larger hole (10.16 cm diameter). Figure 2 shows a horizontal cut of a standard fuel element, as modeled in MCNP, at different levels: in the middle of the block where all the fuel and coolant channels are visible, right below the dowels and at the bottom where the fuel holes are closed. The dowels are modeled as in the core when fuel pins are inserted.

Figure 3 shows similar views but for a RSC/control element. Table 1 summarizes all the fuel and control elements design data provided by General Atomic (GA).

Table 1 Fuel blocks design data

Component	Characteristic	Value
Fuel element	Total fuel holes	210
	Fuel holes under dowels	24
	Fuel hole diameter [cm]	1.270
	Fuel hole length [cm]	78.1558
	Fuel hole length under the dowels [cm]	75.2602
	Large coolant holes	102
	Small coolant holes	6
	Large coolant hole diameter [cm]	1.5875
	Small coolant hole diameter [cm]	1.270
	Fuel/coolant holes pitch [cm]	1.8796
	FBP holes	6
	FBP hole diameter [cm]	1.270
	FBP hole length [cm]	78.1558
	FBP rods (average)	5
	FBP rod diameter [cm]	1.143
	FBP rod length [cm]	72.136
	Dowels	4
	Dowels diameter [cm]	4.445
	Flat-to-flat distance [cm]	36.0
	Gap between elements [cm]	0.1
	Height [cm]	79.3
RSC element	Total fuel holes	186
	Fuel holes under the dowels	24
	Large coolant holes	88
	Small coolant holes	7
	RSC hole diameter [cm]	9.525
	RSC hole offset [cm]	9.75614
Control element	Total fuel holes	186
	Fuel holes under the dowels	24

	Large coolant holes	88
	Small coolant holes	7
	Control rod hole diameter [cm]	10.16
	RSC hole offset [cm]	9.75614
Fuel compact	Diameter [cm]	1.2446
	Length [cm]	4.928
	Compacts per fuel hole	15
	Compacts per fuel hole under the dowel	14
TRISO particle	Kernel diameter [cm]	0.0200
	Buffer thickness [cm]	0.0120
	IPyC coating thickness [cm]	0.0035
	SiC coating thickness [cm]	0.0035
	OPyC coating thickness [cm]	0.0040
	Packing fraction [%]	18

Fuel, RCS and control elements are arranged in the core as shown in Figure 4. There are a total of 12 control elements in the core plus 18 in the reflector. The core also hosts 11 RCS. The elements are separated by 1 mm gap to allow refueling. A 120 cm thick graphite reflector is modeled at the top and the bottom of the core.

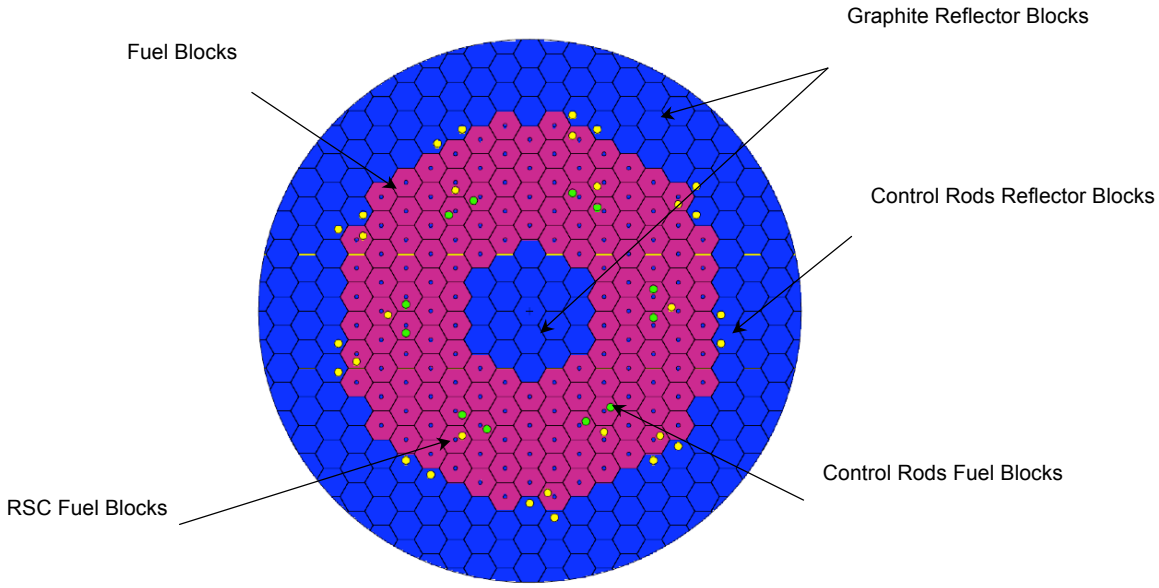

Figure 4 Core horizontal cross section

The fuel particles are discretely modeled to capture the double heterogeneity effects (Figure 5) but in order to save computational time the fuel particle coatings are homogenized into a single layer (Figure 5). The TRISO particles are dispersed in the fuel compacts in a simple cubic structure (Figure 6). It has been shown by many different

evaluations that using a single homogenized coating and using an ordered distribution of fuel kernels rather than a random one, negligibly affect the MCNP calculation results.

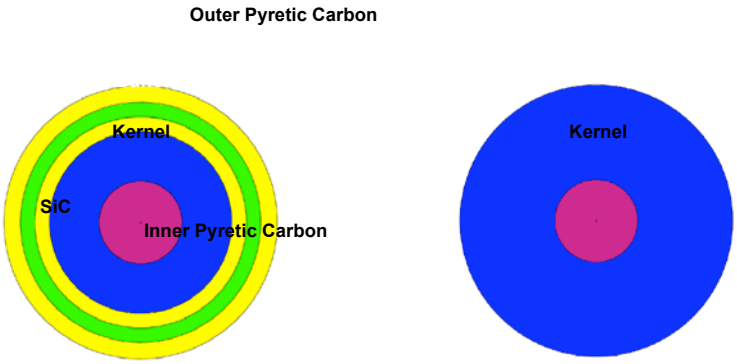

Figure 5 TRISO fuel particle (left) and simplified model with a single homogenized coating (right)

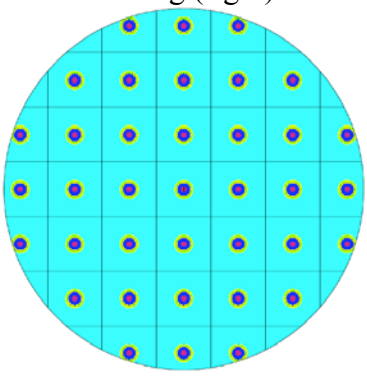

Figure 6 Fuel compact horizontal cross section with TRISO particles distributed according to a simple cubic lattice

2.2 Materials

Table 2 defines all the materials utilized for the different core components. The fuel is $TRUO_2$ where the TRU is obtained from PWR spent fuel assuming 50 GWd/tHM burnup and 5 years of cooling and assuming that Cm is removed to simplify the fuel fabrication. The initial TRU vector is given in Table 3. Nuclear grade graphite H-541 is utilized for the blocks and for all the other graphite components.

Table 2 Core materials property [1]

Material	Composition	Density [g/cm^3]
Fuel	$TRUO_2$	10.36
Carbon Buffer	C	1.00
Pyretic Carbon	C	1.87
SiC	SiC	3.20
Graphite (H-451)	C	1.74

Coolant	He	$3.207 \cdot 10^{-3}$

Table 3 TRU composition – from PWR spent fuel after 50 GWd/tHM burnup, 5 years cooling and Cm removal

Nuclide	Weight Fraction [%]
^{237}Np	6.8
^{238}Pu	2.9
^{239}Pu	49.5
^{240}Pu	23.0
^{241}Pu	8.8
^{242}Pu	4.9
^{241}Am	2.8
^{242m}Am	0.02
^{243}Am	1.4

The core is modeled at a uniform temperature of 1200 K, the radial reflector (inner and outer) at 900 K, while the axial reflector temperature is set at 1200 K for the top and 900 K for the bottom. The coolant is He; it is assumed to be at a pressure of 7 MPa [1]. The corresponding density has been calculated at the average temperature of 1050 K between inlet and outlet. The MCNP model utilizes actual temperature dependent cross sections and scattering kernels for all materials.

2.3 Depletion Model

The MCNP model was set so that it could be utilized in MOCUP for the depletion analysis accounting for a four-batch fuel management scheme with axial and radial shuffling (32 depletion zones). The model can be easily adapted to different fuel management schemes. The radial fuel shuffling scheme is given in Figure 7: the fresh fuel is inserted in the third ring; after the first cycle it is moved to the outer ring, after the second cycle it is moved into the second ring and finally into the inner ring. This radial fuel shuffling is coupled with an axial shuffling as described in Figure 8.

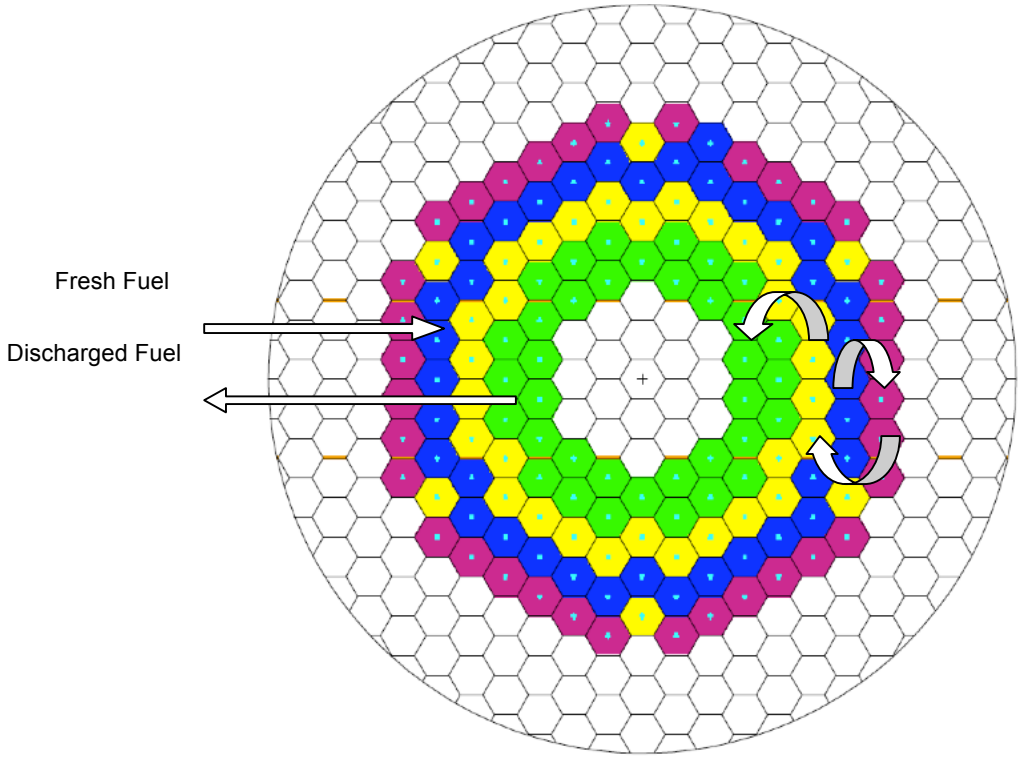

Figure 7 Four-batch radial fuel shuffling scheme

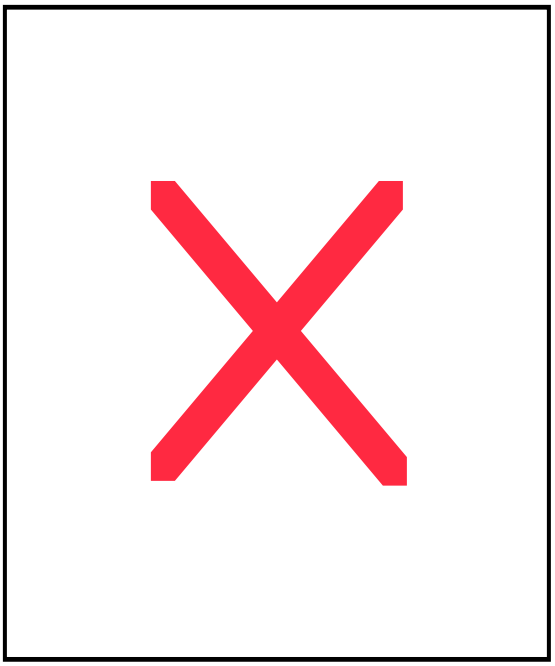

Figure 8 Four-batch axial fuel shuffling scheme

2.4 References

[1] Kim, T.K., Taiwo, T.A., Hill, R.N., Yang, W.S., Venneri, F., "A Feasibility Study of Reactor-Based Deep-Burn Concepts", ANL-AFCI-155, 2005

3. Maximum Achievable Burnup in Deep Burn Modular Helium-cooled Reactor

3.1 Introduction

This study investigates the effects of axial shuffling on the maximum achievable burnup in a deep burn modular helium reactor (DB-MHR). Maximum achievable burnup, reactivity swing, discharge composition, and power distribution in different axial shuffling schemes are compared to a base case without axial shuffling.

3.2 Assumptions

Tables 4 to Table 6 summarize the parameters assumed for, respectively, the fuel composition, TRISO particle geometry, and full core geometry.

Table 4. Fuel composition

Nuclide	Weight Fraction
Np-237	6.8
Pu-238	2.9
Pu-239	49.5
Pu-240	23.0
Pu-241	8.8
Pu-242	4.9
Am-241	2.8
Am-242m	0.02
Am-243	1.4

Table 5. TRISO particle geometry

Layer	Density (g/cc)	Dimension
Fuel Kernel	10.35	200 μm Diameter
Buffer	1.00	120 μm Thickness
Inner PyC	1.87	35 μm Thickness
Silicon Carbide	3.2	40 μm Thickness
Outer PyC	1.87	35 μm Thickness
Matrix	1.74	-

Table 6. Full core parameters

Parameter	Value
Axial Regions	10
Height of Axial Regions	79.3 cm
Initial Heavy Metal Per Axial Region	127 kg

Under these assumptions the full core DB-MHR will have 1.27 tons of heavy metal at the beginning of life (BOL).

The MCNP5 model is coupled to ORIGEN depletion analysis software using MOCUP. The 10 axial fuel elements are assumed to be grouped into 5 axially symmetric depletion zones as shown in Figure 9. 40 day cooling periods are assumed between irradiation periods with axial shuffling.

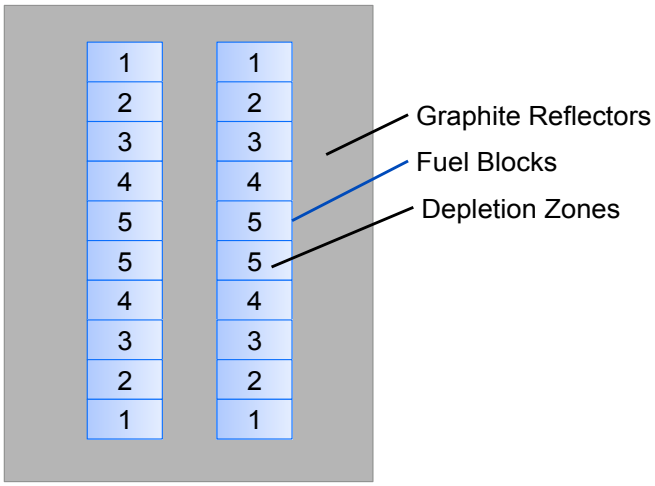

Figure 9. Axially symmetry depletion zones

3.3 Results without fuel shuffling

We define the maximum achievable burnup as the burnup at which the k_{eff} in the DB-MHR system becomes less than one. Figure 10 presents k_{eff} in the DB-MHR without shuffling as a function of burnup. It is found that the maximum attainable burnup is 44.4% FIMA corresponding to 915 EFPD of operation and fuel discharged at 432 GWd/MT.

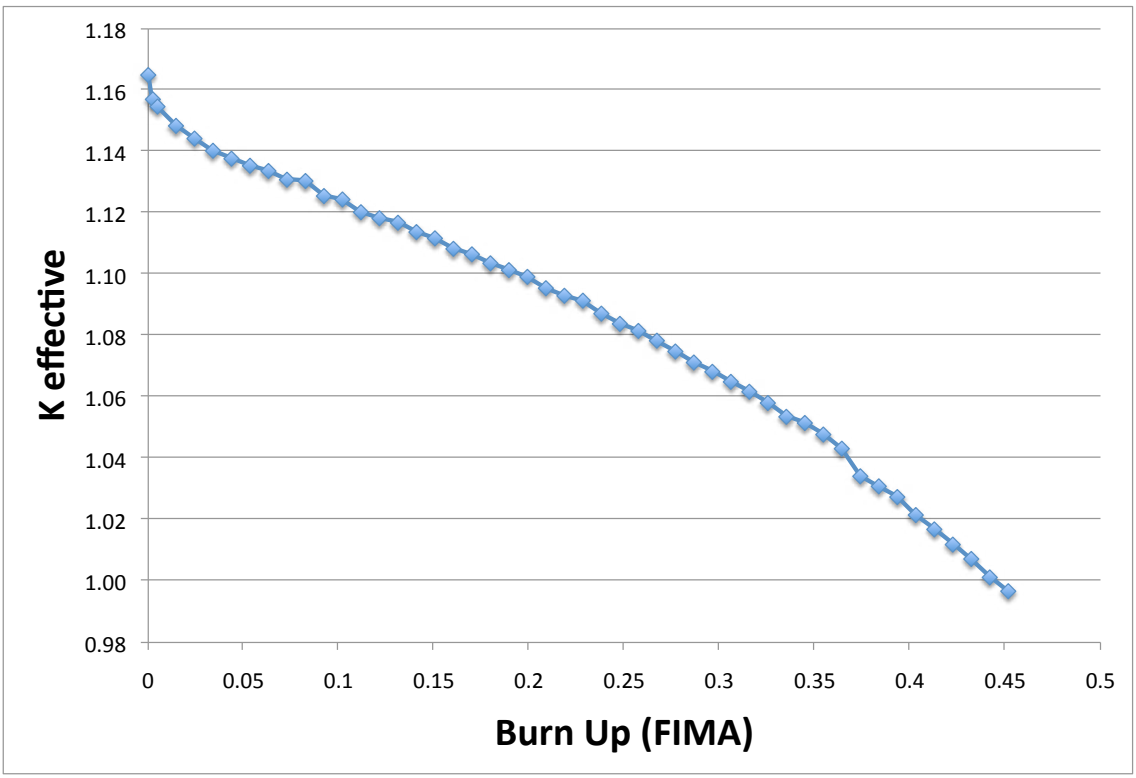

Figure 10. k_{eff} evolution in the DB-MHR without fuel shuffling

The isotopic composition of the DB-MHR in each depletion zone at the end of life is given in Table 7. The initial composition is given at the left column in the table. The regions numbers are those defined in Figure 9.

Table 7. Composition (Metric Tons) of each axial region of the DB-MHR without shuffling

-	fresh	burned 1x	burned 1x	burned 1x	burned 1x	burned 1x	-
nuclide	core	region 1	region 2	region 3	region 4	region 5	Consumed
U 233	-	0.00E+00	0.00E+00	0.00E+00	0.00E+00	0.00E+00	-
U 234	-	1.89E-04	1.88E-04	1.85E-04	1.82E-04	1.77E-04	-
U 235	-	2.90E-05	2.89E-05	2.88E-05	2.76E-05	2.32E-05	-
U 236	-	1.29E-05	1.30E-05	1.31E-05	1.33E-05	1.41E-05	-
U 237	-	2.24E-08	2.34E-08	2.55E-08	2.54E-08	2.13E-08	-
U 238	-	7.51E-08	7.45E-08	7.31E-08	7.03E-08	6.74E-08	-
NP 237	8.54E-02	9.57E-03	9.63E-03	9.85E-03	1.04E-02	1.15E-02	**88.06%**
NP 239	-	2.90E-08	3.14E-08	3.31E-08	2.87E-08	2.02E-08	-
PU 238	3.66E-02	1.52E-02	1.52E-02	1.51E-02	1.47E-02	1.38E-02	**59.54%**
PU 239	6.27E-01	1.11E-02	1.15E-02	1.29E-02	1.73E-02	2.45E-02	**97.54%**
PU 240	2.93E-01	3.14E-02	3.18E-02	3.31E-02	3.64E-02	4.48E-02	**87.86%**
PU 241	1.12E-01	2.91E-02	2.95E-02	3.04E-02	3.25E-02	3.26E-02	**72.57%**
PU 242	6.28E-02	2.26E-02	2.24E-02	2.19E-02	2.07E-02	1.91E-02	**66.04%**
AM 241	3.58E-02	2.71E-03	2.76E-03	2.91E-03	3.38E-03	4.10E-03	**91.13%**
AM 242*	2.56E-04	7.78E-06	8.24E-06	8.87E-06	9.04E-06	8.30E-06	**96.71%**
AM 243	1.80E-02	5.55E-03	5.54E-03	5.46E-03	5.27E-03	4.88E-03	**70.37%**
CM 242	-	1.56E-03	1.58E-03	1.61E-03	1.58E-03	1.44E-03	-
CM 243	-	4.36E-05	4.33E-05	4.21E-05	3.81E-05	2.89E-05	-
CM 244	-	5.10E-03	5.06E-03	4.89E-03	4.43E-03	3.44E-03	-
CM 245	-	4.68E-04	4.64E-04	4.45E-04	3.96E-04	2.61E-04	-
Plutonium	1.13E+00	1.09E-01	1.10E-01	1.13E-01	1.22E-01	1.35E-01	**47.88%**
Heavy Metal	1.27E+00	1.35E-01	1.36E-01	1.39E-01	1.47E-01	1.61E-01	**43.51%**

Notice that the material in the center of the reactor (depletion zone 1) was burned more deeply than the material in the periphery of the reactor (depletion zone 2).

The Normalized Power distribution is plotted in Figure 11. In this plot, the axial regions correspond to the depletion zones shown in Figure 9, the line y=0 corresponds to the center of the reactor and likewise whereas the line y=5 corresponds to the top and bottom of the reactor. It is found that at BOL the power is peaked toward the center of the reactor but is pretty flat at End of Life (EOL).

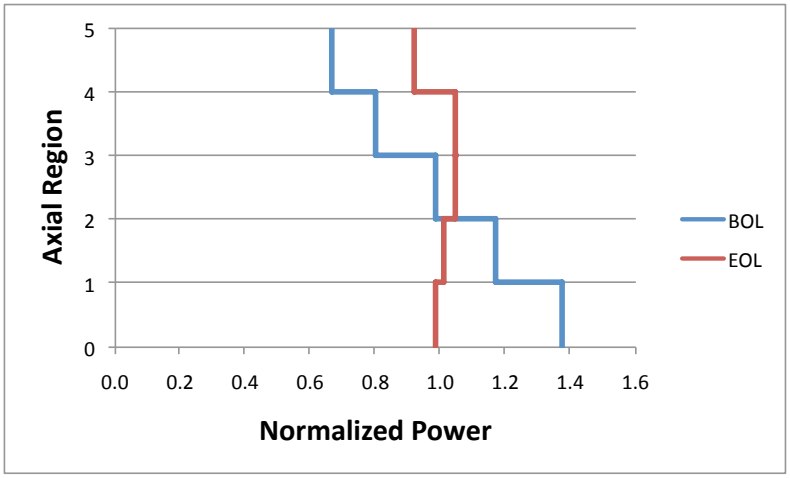

Figure 11. Power Distribution in DB-MHR at BOL and EOL.

3.4 Results with axial shuffling

Three different axial shuffling schemes were investigated. These schemes are presented in Figure 12.

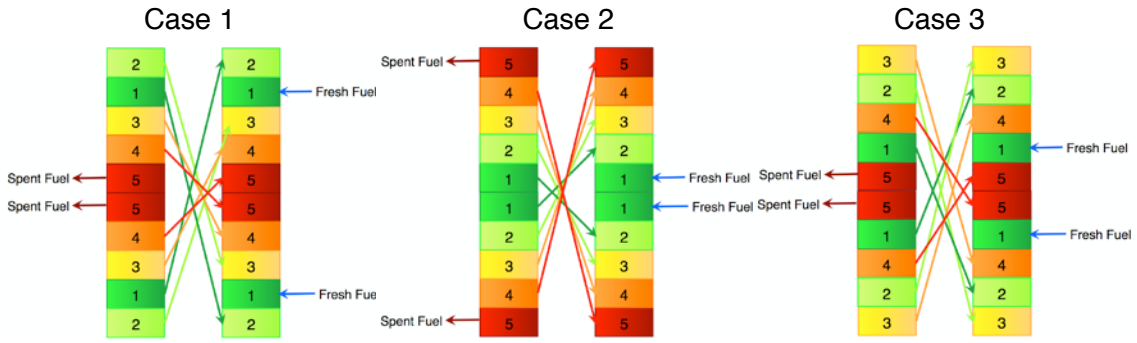

Figure 12. Axial shuffling schemes examined for the DB-MHR

Case 1 places the most burned fuel at the center of the reactor where most of the actinides were burned in the case without shuffling. Case 2 takes advantage of the low leakage probability in the center of the core by placing the freshest fuel there. Finally, Case 3 attempts to place high burnup fuel next to low burnup fuel so that excess neutrons from low burnup regions will drive the high burnup regions.

To reach equilibrium compositions multiple shuffling iterations were preformed. The composition of the reactor is assumed to be converged when the concentration of the actinides in the discharge fuel do not change by more than 1% between successive iterations. The cycle is calculated iteratively. Figure 13 illustrates the composition convergence process. The "normalized composition" of nuclide, N, at iteration, j, shown in the figure, is N_j/N_{j-1}.

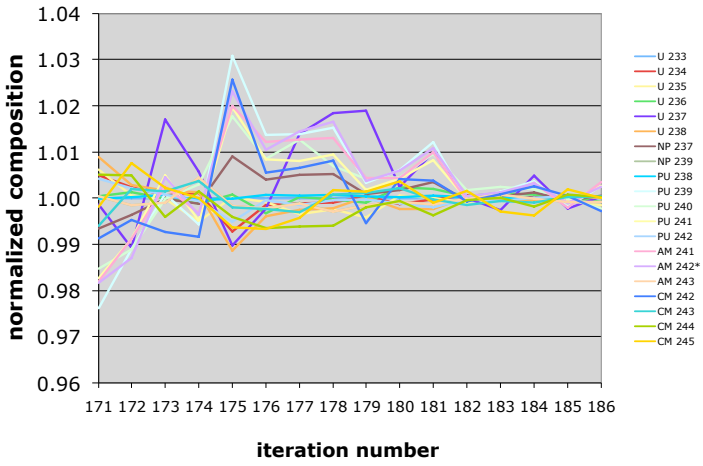

Figure 13. Illustration of the discharge composition convergence in shuffling scheme of Case 3

The equilibrium cycle length is also iterated upon. If k_{eff} at EOC is less than 1 then the cycle length is shortened. Conversely, if k_{eff} at EOC is greater than 1 the cycle length is increased. The maximum achievable burnup corresponds to the cycle length for which the EOC k_{eff} equals 1.0. Figure 14 plots k_{eff} evolution towards the EOC for each of the three axial shuffling schemes examined. The corresponding maximum achievable burnups are compared in Table 7.

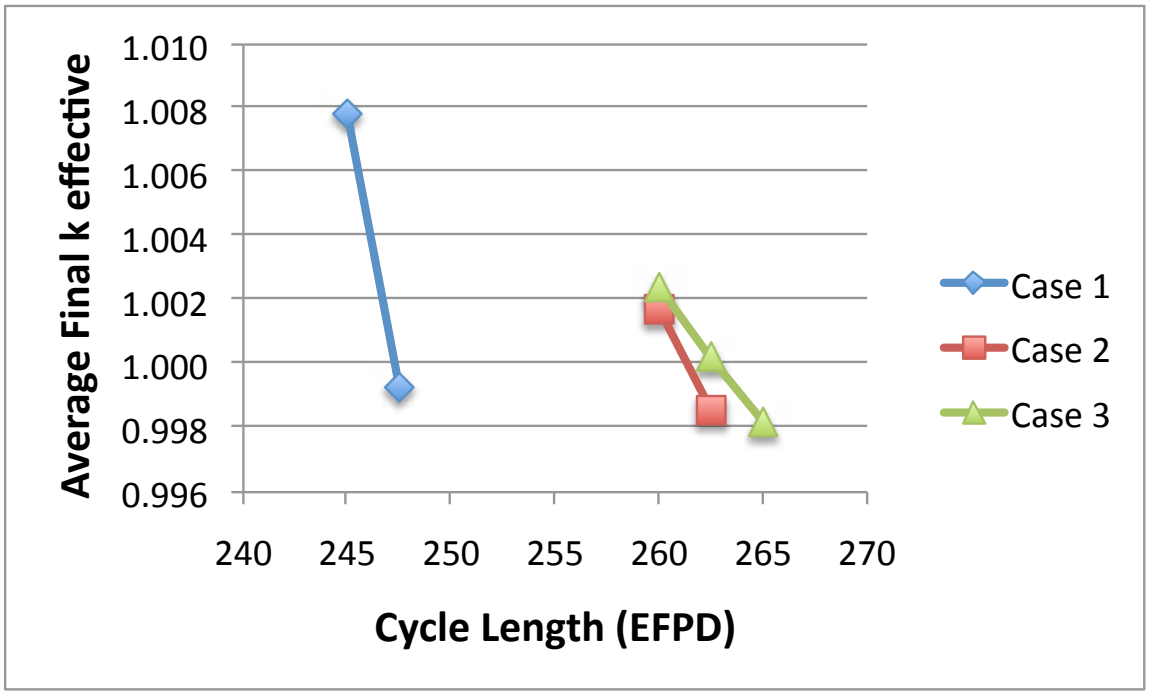

Figure 14. Converged k_{eff} vs cycle length in the vicinity of EOC for various axial shuffling schemes

Table 7. Maximum achievable burnup with axial shuffling.

Case	Cycle Length	Burnup (EFPD)	Burnup (GWd/MT)	Burnup (FIMA)
1	247.3	1236.5	583.9	59.8%
2	261.3	1306.5	616.9	63.1%
3	263.4	1317.0	621.9	63.6%

The k_{eff} history for five iterations are plotted for the three axial shuffling cases with various cycle lengths in Figure 15 to Figure 17. The reactivity swing in each of the cases is compared in Table 8. The reactivity swing is weakly dependent on the axial shuffling scheme, where Case 2 has a very large reactivity swing and Case 3 has the smallest reactivity swing.

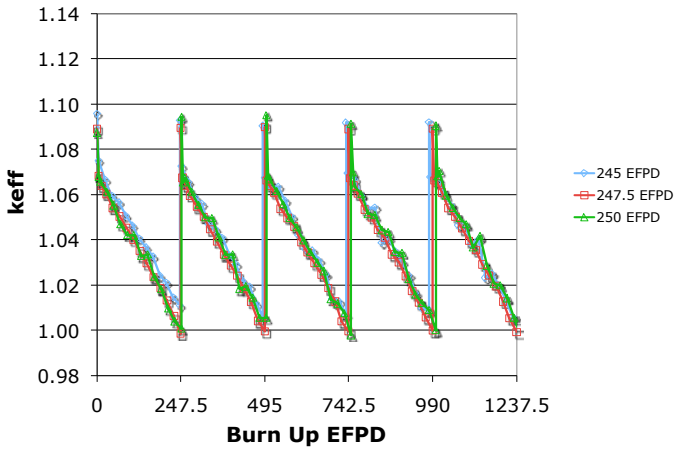

Figure 15. k_{eff} of DB-MHR with Case 1 axial shuffling scheme

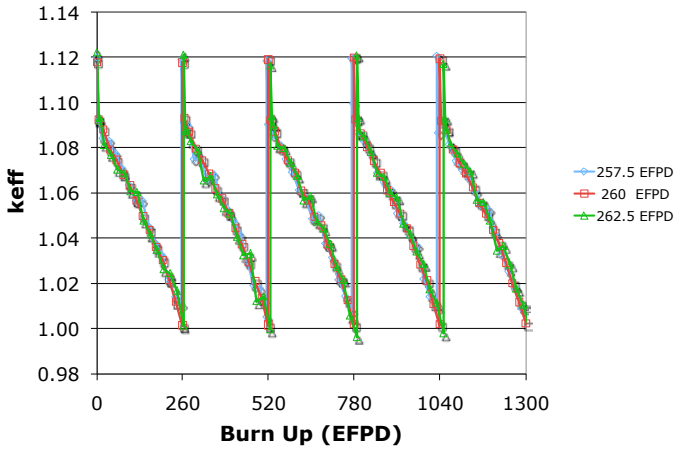

Figure16. k_{eff} of DB-MHR with Case 2 axial shuffling scheme

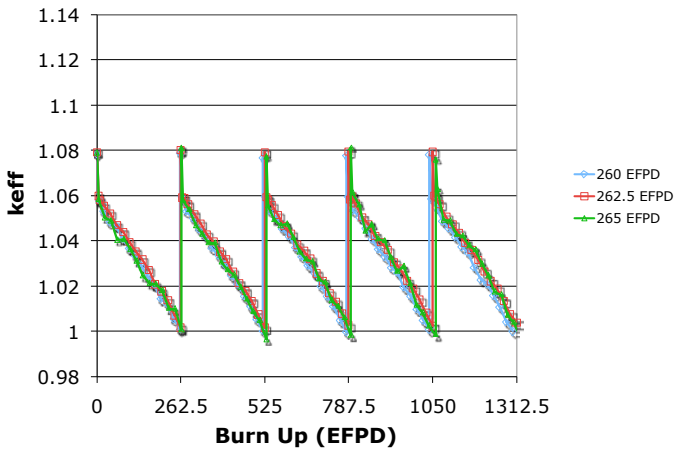

Figure 17. k_{eff} of DB-MHR with Case 3 axial shuffling configuration

Table 8. Estimated reactivity swing over irradiation cycle

Case	Decrease in k_{eff}
1	8.9%
2	10.8%
3	7.9%

The actinides composition vector at EOC are given in Table 9 to Table 11 for the three shuffling schemes. Table 12 compares the discharged actinides composition vector for the different axial shuffling schemes.

Table 9. Composition vector of heavy metal in fuel (in tons) at each burnup level for Case 1 shuffling scheme assuming 247.5 days cycle length

Axial Shuffling Scheme: Case 1							
Burnup	fresh	1x burned	2x burned	3x burned	4x burned	5x burned	-
nuclide	region 1	region 2	region 3	region 4	region 5	discharge	Consumped
U 233	-	0.00E+00	0.00E+00	0.00E+00	0.00E+00	0.00E+00	-
U 234	-	5.30E-05	1.19E-04	1.95E-04	2.81E-04	3.59E-04	-
U 235	-	4.85E-06	1.51E-05	2.56E-05	3.24E-05	3.71E-05	-
U 236	-	4.45E-06	8.12E-06	1.11E-05	1.34E-05	1.50E-05	-
U 237	-	1.26E-09	1.31E-09	9.98E-10	7.07E-10	5.07E-09	-
U 238	-	2.07E-08	4.88E-08	8.23E-08	1.19E-07	1.52E-07	-
NP 237	1.71E-02	1.32E-02	1.02E-02	8.47E-03	7.70E-03	7.34E-03	**57.02%**
NP 239	-	3.80E-09	4.60E-09	5.16E-09	5.34E-09	7.15E-09	-
PU 238	7.31E-03	1.13E-02	1.43E-02	1.57E-02	1.62E-02	1.64E-02	**-124.04%**
PU 239	1.25E-01	4.90E-02	1.47E-02	5.67E-03	3.69E-03	3.07E-03	**97.55%**
PU 240	5.85E-02	5.16E-02	3.61E-02	2.48E-02	2.05E-02	1.86E-02	**68.27%**
PU 241	2.25E-02	3.52E-02	3.18E-02	2.37E-02	1.87E-02	1.62E-02	**27.86%**
PU 242	1.26E-02	1.59E-02	2.13E-02	2.51E-02	2.69E-02	2.76E-02	**-119.96%**
AM 241	7.15E-03	4.33E-03	2.69E-03	2.01E-03	1.98E-03	2.08E-03	**70.88%**
AM 242*	5.13E-05	9.71E-05	5.61E-05	3.83E-05	3.40E-05	3.44E-05	**32.97%**
AM 243	3.61E-03	4.41E-03	5.35E-03	6.00E-03	6.20E-03	6.28E-03	**-74.24%**
CM 242	-	1.54E-03	1.58E-03	1.14E-03	6.69E-04	4.57E-04	-
CM 243	-	2.56E-05	4.84E-05	4.98E-05	4.55E-05	4.17E-05	-
CM 244	-	2.35E-03	4.59E-03	6.03E-03	6.56E-03	6.75E-03	-
CM 245	-	1.41E-04	4.05E-04	5.53E-04	5.69E-04	5.67E-04	-
Plutonium	2.26E-01	1.63E-01	1.18E-01	9.50E-02	8.60E-02	8.19E-02	**63.81%**
Heavy Metal	2.54E-01	1.89E-01	1.43E-01	1.20E-01	1.10E-01	1.06E-01	**58.31%**

Table 10. Composition vector of heavy metal in fuel (in tons) at each burnup level for Case 2 shuffling scheme assuming 260 days cycle length

Axial Shuffling Scheme: Case 2							
Burnup	fresh	1x burned	2x burned	3x burned	4x burned	5x burned	-
nuclide	region 1	region 2	region 3	region 4	region 5	discharge	Consumped
U 233	-	0.00E+00	0.00E+00	0.00E+00	0.00E+00	0.00E+00	-
U 234	-	5.69E-05	1.35E-04	2.23E-04	3.20E-04	4.08E-04	-
U 235	-	6.66E-06	1.79E-05	2.57E-05	3.02E-05	3.24E-05	-
U 236	-	4.13E-06	7.20E-06	9.43E-06	1.12E-05	1.25E-05	-
U 237	-	1.40E-09	9.15E-10	5.43E-10	3.96E-10	1.37E-09	-
U 238	-	2.46E-08	6.30E-08	1.05E-07	1.48E-07	1.85E-07	-
NP 237	1.71E-02	1.11E-02	7.80E-03	6.66E-03	6.36E-03	6.35E-03	**62.83%**
NP 239	-	4.36E-09	5.32E-09	5.62E-09	5.63E-09	5.83E-09	-
PU 238	7.31E-03	1.29E-02	1.52E-02	1.56E-02	1.57E-02	1.59E-02	**-116.76%**
PU 239	1.25E-01	2.41E-02	4.18E-03	2.37E-03	2.14E-03	2.13E-03	**98.30%**
PU 240	5.85E-02	3.99E-02	2.04E-02	1.44E-02	1.34E-02	1.35E-02	**76.87%**
PU 241	2.25E-02	3.59E-02	2.08E-02	1.36E-02	1.15E-02	1.10E-02	**51.22%**
PU 242	1.26E-02	1.92E-02	2.64E-02	2.86E-02	2.91E-02	2.92E-02	**-132.46%**
AM 241	7.15E-03	2.78E-03	1.33E-03	1.13E-03	1.33E-03	1.66E-03	**76.80%**
AM 242*	5.13E-05	6.33E-05	2.50E-05	1.92E-05	2.01E-05	2.27E-05	**55.73%**
AM 243	3.61E-03	5.06E-03	6.18E-03	6.53E-03	6.54E-03	6.53E-03	**-81.22%**
CM 242	-	2.09E-03	1.45E-03	7.26E-04	3.35E-04	1.79E-04	-
CM 243	-	5.39E-05	6.43E-05	5.39E-05	4.76E-05	4.49E-05	-
CM 244	-	4.05E-03	6.79E-03	7.75E-03	7.79E-03	7.59E-03	-
CM 245	-	3.52E-04	6.18E-04	6.23E-04	6.09E-04	5.95E-04	-
Plutonium	2.26E-01	1.32E-01	8.70E-02	7.45E-02	7.18E-02	7.17E-02	**68.31%**
Heavy Metal	2.54E-01	1.58E-01	1.11E-01	9.84E-02	9.54E-02	9.53E-02	**62.52%**

Table 11. Composition vector of heavy metal in fuel (in tons) at each burnup level for Case 3 shuffling scheme assuming 262.5 days cycle length

Axial Shuffling Scheme: Case 3							
Burnup	fresh	1x burned	2x burned	3x burned	4x burned	5x burned	-
nuclide	region 1	region 2	region 3	region 4	region 5	discharge	Consumped
U 233	0.00E+00	0.00E+00	0.00E+00	0.00E+00	0.00E+00	0.00E+00	-
U 234	1.06E-23	5.52E-05	1.25E-04	1.97E-04	2.81E-04	3.48E-04	-
U 235	1.07E-23	4.88E-06	1.40E-05	2.96E-05	4.10E-05	5.29E-05	-
U 236	1.07E-23	4.77E-06	8.90E-06	1.24E-05	1.54E-05	1.80E-05	-
U 237	1.08E-23	1.22E-09	1.31E-09	1.20E-09	7.97E-10	1.65E-08	-
U 238	1.08E-23	2.11E-08	4.75E-08	8.25E-08	1.22E-07	1.59E-07	-
NP 237	1.71E-02	1.38E-02	1.13E-02	8.75E-03	7.34E-03	6.20E-03	**63.71%**
NP 239	1.08E-23	3.69E-09	4.26E-09	5.06E-09	5.45E-09	2.10E-08	-
PU 238	7.31E-03	1.08E-02	1.37E-02	1.56E-02	1.63E-02	1.59E-02	**-117.59%**
PU 239	1.25E-01	5.91E-02	2.45E-02	6.81E-03	3.15E-03	2.06E-03	**98.36%**
PU 240	5.85E-02	5.29E-02	4.26E-02	2.63E-02	1.80E-02	1.23E-02	**78.98%**
PU 241	2.25E-02	3.48E-02	3.40E-02	2.55E-02	1.72E-02	1.12E-02	**50.11%**
PU 242	1.26E-02	1.50E-02	1.91E-02	2.44E-02	2.74E-02	2.92E-02	**-132.51%**
AM 241	7.15E-03	4.91E-03	3.64E-03	2.16E-03	1.60E-03	1.06E-03	**85.24%**
AM 242*	5.13E-05	1.07E-04	7.68E-05	4.31E-05	2.90E-05	1.97E-05	**61.58%**
AM 243	3.61E-03	4.29E-03	4.95E-03	5.88E-03	6.34E-03	6.65E-03	**-84.49%**
CM 242	1.10E-23	1.30E-03	1.37E-03	1.37E-03	9.00E-04	7.47E-04	-
CM 243	1.10E-23	1.94E-05	3.67E-05	4.76E-05	4.46E-05	3.77E-05	-
CM 244	1.11E-23	2.02E-03	3.70E-03	5.78E-03	6.96E-03	7.98E-03	-
CM 245	1.11E-23	1.09E-04	3.03E-04	5.37E-04	6.00E-04	6.00E-04	-
Plutonium	2.26E-01	1.73E-01	1.34E-01	9.87E-02	8.21E-02	7.07E-02	**68.74%**
Heavy Metal	2.54E-01	1.99E-01	1.59E-01	1.24E-01	1.06E-01	9.46E-02	**62.78%**

Table12. Discharge composition (in tons) of DB-MHR with different shuffling cases compared to the case without axial shuffling

Case	No Shuffling	1	2	3
EFPD	910	1237.5	1300	1312.5
U 233	0.00E+00	0.00E+00	0.00E+00	0.00E+00
U 234	1.84E-04	3.59E-04	4.08E-04	3.48E-04
U 235	2.75E-05	3.71E-05	3.24E-05	5.29E-05
U 236	1.33E-05	1.50E-05	1.25E-05	1.80E-05
U 237	2.36E-08	5.07E-09	1.37E-09	1.65E-08
U 238	7.21E-08	1.52E-07	1.85E-07	1.59E-07
Np 237	1.02E-02	7.34E-03	6.35E-03	6.20E-03
Np 239	2.85E-08	7.15E-09	5.83E-09	2.10E-08
Pu 238	1.48E-02	1.64E-02	1.59E-02	1.59E-02
Pu 239	1.54E-02	3.07E-03	2.13E-03	2.06E-03
Pu 240	3.55E-02	1.86E-02	1.35E-02	1.23E-02
Pu 241	3.08E-02	1.62E-02	1.10E-02	1.12E-02
Pu 242	2.13E-02	2.76E-02	2.92E-02	2.92E-02
Am 241	3.17E-03	2.08E-03	1.66E-03	1.06E-03
Am 242*	8.45E-06	3.44E-05	2.27E-05	1.97E-05
Am 243	5.34E-03	6.28E-03	6.53E-03	6.65E-03
Cm 242	1.55E-03	4.57E-04	1.79E-04	7.47E-04
Cm 243	3.92E-05	4.17E-05	4.49E-05	3.77E-05
Cm 244	4.58E-03	6.75E-03	7.59E-03	7.98E-03
Cm 245	4.07E-04	5.67E-04	5.95E-04	6.00E-04
Plutonium Destruction	8.96E-01	9.28E-01	9.37E-01	9.37E-01
Increase v. No Shuff	-	3.56E-02	4.56E-02	4.66E-02
Fissile Pu Destruction	6.93E-01	7.20E-01	7.26E-01	7.26E-01
Increase v. No Shuff	-	3.89E-02	4.79E-02	4.76E-02
Heavy Metal Destruction	4.35E-01	5.83E-01	6.25E-01	6.28E-01
Increase v. No Shuff	-	3.40E-01	4.37E-01	4.43E-01

The axial shuffling scheme has a large impact on the axial power distribution in the DB-MHR. The BOL coarse axial power distributions corresponding to each shuffling scheme is shown in Figure 18 to Figure 20 The positions in the figures correspond to the axial configuration presented in Figure 9 where the line y=0 represents the axial center of the core. The plots give the normalized average power per fuel element. The maximum power peaking factor at BOL and EOL is summarized in Table 13 for each axial shuffling scheme.

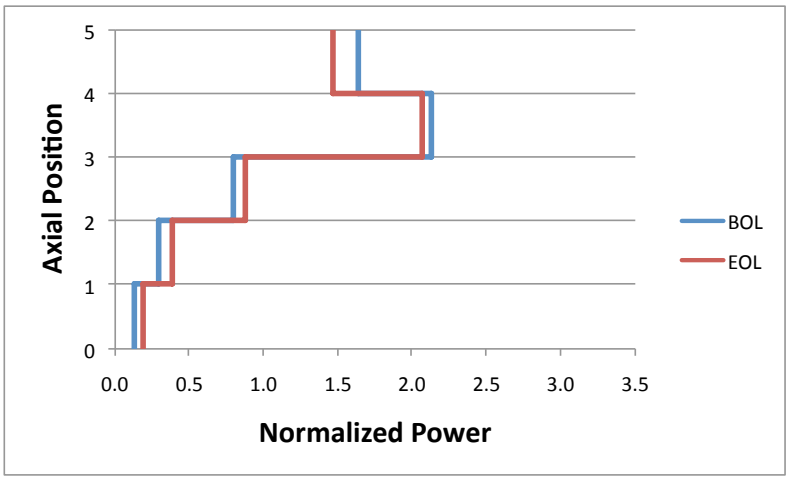

Figure 18. Coarse normalized axial power distribution in DB-MHR with Case 1 shuffling scheme

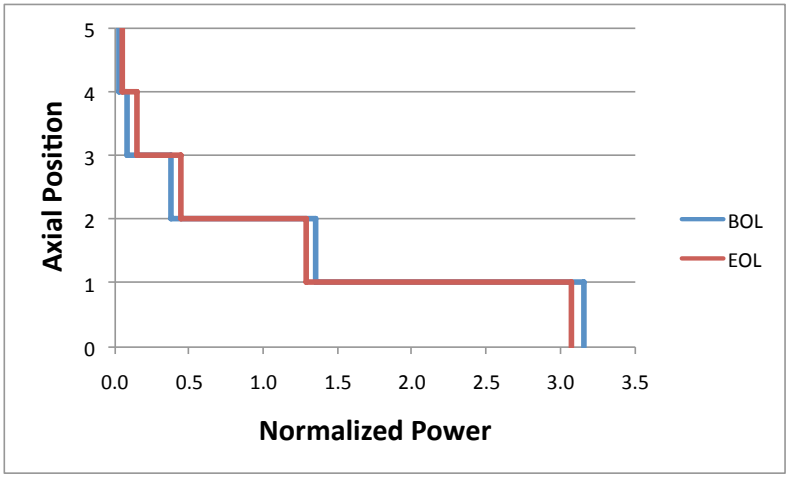

Figure19. Coarse normalized axial power distribution in BD-MHR with Case 2 shuffling scheme

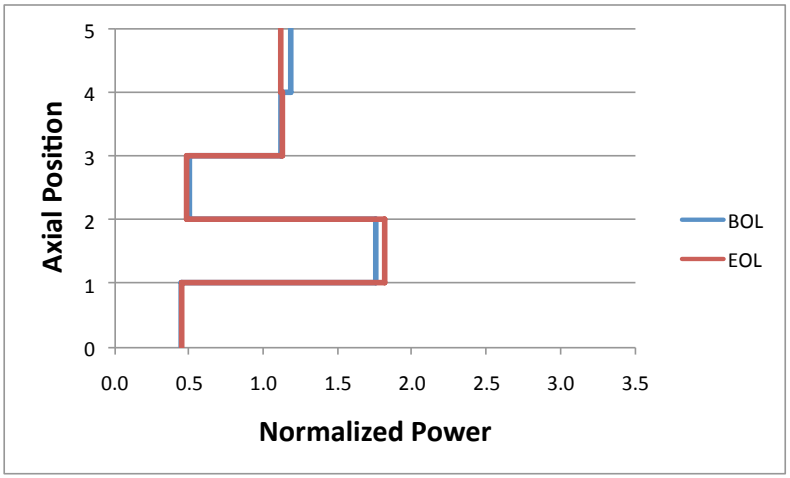

Figure20. Coarse normalized axial power distribution in BD-MHR with Case 3 shuffling scheme

Table13. Maximum axial power peaking factors at beginning and end of life for different shuffling schemes

Case	Maximum Power Peaking Factor at BOL	Maximum Power Peaking Factor at EOL
No Shuffling	1.37	1.05
1	2.13	2.03
2	3.15	3.07
3	1.75	1.81

Unlike other parameters, switching to axial shuffling decrease performance with respect to power peaking factors. However, using the Case 3 axial shuffling configuration best mitigates power peaking.

3.5 Summary

Axial shuffling increases the maximum achievable burnup in the DB-MHR from 432 GWd/MT to 622 GWd/MT, an increase of 44%. Furthermore, the burnup reactivity swing over the cycle decreases from 16.5% to only 7.9%, a decrease of 52%. The fraction of all fissile plutonium isotopes destroyed increases by 4.8% from no shuffling to axial shuffling. However, the maximum power peaking factor increases from a maximum of 1.37 at BOL in the case without axial shuffling to 1.81 at EOL with case 3 axial shuffling. Case 3 is the preferred axial shuffling scheme – it offers the highest burnup, lowest reactivity swing, most actinides destroyed and the lowest power peaking factor.

4. Comparison of DB-MHR with Alternative TRISO Fueled Core Designs

4.1 Introduction

The University of California at Berkeley recently conceived of the PB-AHTR – a Pebble Bed Advanced High Temperature Reactor that is cooled with the liquid salt flibe (LiF-BeF_2) rather than helium [1-3]. Recent experiments have demonstrated that pebble beds can be formed with a liquid salt coolant and pebbles can be recirculated [1]. The PB-AHTR can use the same fuel kernels as the DB-AHTR but can operate them at significantly higher power density due to the enhanced heat transfer coefficients of the flibe coolant. Hence, in this section we are quantifying the burnup attainable from a PB-AHTR and compare it, as well as other characteristics, with those of the DB-MHR.

The analysis was limited to a predefined set of design parameters. The fuel kernel diameter was fixed at 200 μm for both designs as this is the preferred size to be utilized in the DB-MHR in order to maximize incineration of TRU; in larger kernels the spatial self-shielding could prevent a full depletion of the kernel. The coatings thicknesses are as follows – the carbon buffer thickness is120 μm, inner pyrolitic carbon 35 μm, SiC 35 μm, outer pyrolitic carbon 40 μm. The fuel is $TRUO_{1.7}$ with the TRU composition, given in Table 14, corresponding to the spent fuel discharged from LWRs after 50 GWd/tHM burnup, 5 years cooling and complete removal of uranium, curium and fission products [4]. The reactor-specific assumptions are defined in the following sections.

Table 14. Initial TRU composition from LWRs spent fuel after 50 GWd/tHM burnup, 5 years cooling and complete removal of U, Cm and fission products [4].

Nuclide	Weight Fraction (%)
^{237}Np	6.8
^{238}Pu	2.9
^{239}Pu	49.5
^{240}Pu	23.0
^{241}Pu	8.8
^{242}Pu	4.9
^{241}Am	2.8
^{242m}Am	0.02
^{243}Am	1.4

4.2 Attainable burnup of the PB-AHTR

The depletion analysis for the deep-burn PB-AHTR was performed applying the single pebble in equilibrium bed methodology described in Reference [5]. The total core power is 2,400 MW_{th}, the power density is 10.2 MW/m^3 and the core components temperatures were assumed the same as for the design fueled with enriched uranium [5]. The leakage probability was accurately determined using a full core model because the attainable burnup is very sensitive to it. A preliminary value was obtained using all fresh fuel core, and corrected after an equilibrium core composition was established. It was found that the leakage probability has a minimum value for TRISO particles packing factor of about 10%. For larger packing factors it increases due to spectrum hardening and for lower packing factors it increases due to decrease in the core macroscopic absorption cross section. For the range of packing factors of interest in this study the neutron leakage probability is ~3%.

The attainable burnup and TRU incineration fraction were searched varying the graphite-to-heavy metal atom ratio while keeping constant the fuel kernel diameter. The results are summarized in Table 15. It was found that the maximum burnup of 653.5 GWd/tHM and therefore the maximum HM consumption of 66.4% is achieved with C/HM of ~2,500, but in general burnup and HM incineration are only slightly sensitive to the C/HM. Plutonium inventory is reduced by ~74% and its fissile content gets smaller as the neutron spectrum gets softer. The inventory of long-lived ^{237}Np and its precursors (^{241}Pu, ^{241}Np, ^{245}Cm, ^{249}Bk) are reduced by ~58% and their transmutation is particularly sensitive to C/HM because softer spectra can better fission ^{241}Pu.

Table 15. Transmutation properties of the PB-AHTR as a function of TRISO particles packing factor for 200 μm diameter fuel kernels and initial HM load TRU from LWRs spent fuel.

Property	C/HM			
	1684	1993	2439	2746
Packing factor	13%	11%	9%	7%
Initial HM mass (t)	2.75	2.33	1.90	1.69
Neutron flux (n/cm^2-s)	$2.97 \cdot 10^{14}$	$3.20 \cdot 10^{14}$	$3.48 \cdot 10^{14}$	$3.99 \cdot 10^{14}$
Burnup (GWd/tHM)	642.3	650.3	653.5	651.7
Residence time (EFPD)	736	631	518	402
HM consumption (%)	65.2	66.1	66.4	66.2
Pu consumption (%)	73.4	74.2	74.2	72.9
Fissile Pu consumption (%)	88.4	90.2	91.2	92.1
^{237}Np and precursors consumption (%)	41.8	51.5	57.6	62.3

For the design to be feasible, all the reactivity coefficients of a deep-burn PB-AHTR must be negative. The reactivity feedbacks were calculated, using the methodology described in Reference [5], for the core equilibrium composition that was preliminary obtained from the depletion analysis. Table 16 summarizes the results for selected designs. All reactivity coefficients are found negative for under-moderated designs while over-moderated designs have positive coolant temperature and small void reactivity coefficients. The maximum burnup design corresponding to C/HM ~2,500 features all negative reactivity coefficients.

Table 16. Reactivity coefficient of the deep-burn PB-AHTR equilibrium core for selected graphite-to-heavy metal atom ratio.

Reactivity coefficient	C/HM			
	1,684	1,993	2,439	2,746
Fuel temperature (pcm/K)	-1.81	-1.71	-1.51	-1.28
Coolant temperature (pcm/K)	-2.01	-1.56	-0.94	+0.13
Coolant void (pcm/void%)	-55.77	-43.83	-25.83	+3.90
Full coolant void (pcm/void%)	-85.05	-74.09	-54.29	-21.00
Moderator temperature (pcm/K)	-3.94	-4.39	-3.88	-2.93
Moderator + fuel temperature (pcm/K)	-6.11	-5.85	-5.46	-4.31
Moderator + coolant temp (pcm/K)	-6.18	-6.29	-5.23	-3.33

4.2 Attainable burnup of the DB-MHR

The DB-MHR core is composed of hexagonal prismatic fuel blocks that form a pseudo-annular core. Multiple core configurations have been proposed over the years characterized by different number of rings and different shuffling schemes. For this comparison we selected a five rings configuration shown in Figure 21 and four-batch fuel management scheme. The methodology applied for determining the attainable burnup is described in Reference [5]. The leakage probability was estimated using a full core model; its average value between BOL and EOL is found to be ~5%.

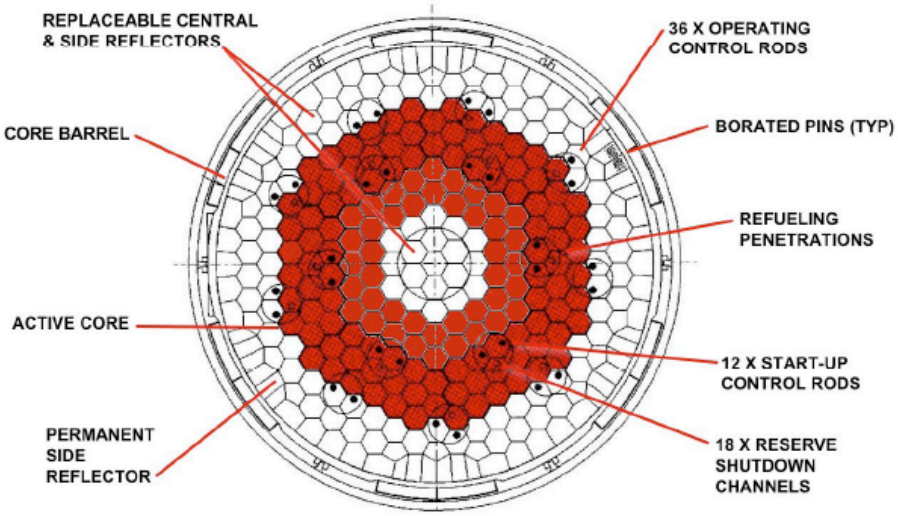

Figure 21 DB-MHR core horizontal view with five fuel element rings [4].

The maximum attainable burnup was searched as a function of C/HM. The results, summarized in Table 17, suggest that the optimal C/HM is ~2,500 corresponding to a TRISO particles packing factor of 14%. As observed for the PB-AHTR, plutonium and HM fractional consumption are not very sensitive to the C/HM ratio; the fissile plutonium consumption increases with softer spectra; ^{237}Np and precursors consumption is more sensitive to the spectrum and is larger for larger C/HM since ^{241}Pu and ^{241}Am fission cross sections increase in soft spectra.

Table 17. Transmutation properties of the DB-MHR as a function of TRISO particles packing factor for 200 μm diameter fuel kernels and initial HM load TRU from LWR spent fuel.

Property	C/HM			
	1,970	2,216	2,533	2,955
Packing factor	18%	16%	14%	12%
Initial HM mass (t)	1.31	1.16	1.02	0.87
Burnup (GWd/tHM)	613.7	618.1	621.3	617.4
Residence time (EFPD)	1336	1196	1052	896
HM consumption (%)	62.45	63.01	63.24	62.84
Pu consumption (%)	69.24	69.35	69.49	68.58
Fissile Pu consumption (%)	89.06	90.18	91.16	91.68
^{237}Np and precursors consumption (%)	47.74	54.11	58.44	61.28

4.3 Comparison

The PB-AHTR and DB-MHR maximum burnup designs are compared in Table 18 in terms of the overall transmutation performance and final waste properties. It is found that the attainable burnups are similar for the two systems, only ~30 GWd/tHM larger for the PB-AHTR that translates into a ~3% (absolute) larger heavy metal consumption.

Table 18. PB-AHTR and DB-MHR transmutation properties

Property	PB-AHTR	DB-MHR
Total core power (MW_{th})	2,400	600
Power density (MW/m^3)	10.2	4.68
Initial HM mass (t)	1.90	1.02
C/HM	2,439	2,533
Leakage probability (%)	3	5
Burnup (GWd/tHM)	653.5	621.3
Residence time (EFPD)	518	1052
HM consumption (%)	66.4	63.2
Pu consumption (%)	74.2	69.5
Fissile Pu consumption (%)	91.2	91.2
^{237}Np and precursors consumption (%)	57.6	58.4

The somewhat improved transmutation performance of the PB-AHTR is due to: (1) the continuous refuelling mode of the pebble bed reactor versus the batch mode of the prismatic fuel reactor; (2) the lower leakage probability of the PB-AHTR. These advantages more than compensate for the intrinsic disadvantage for the PB-AHTR – the

relatively large coolant absorption probability. Table 19 and Table 20 compare the fraction of neutron absorption in the different constituents of the two cores at, respectively, BOL and EOL. The relatively large difference in fractional absorption at EOL is due to spectral differences.

Table 19. Comparison of fractional absorption in core components at BOL

System	PB-AHTR	DB-HTR
Fuel	96.83%	99.11%
Coatings	0.16%	0.15%
Matrix	0.22%	0.19%
Pebble shell/blocks	0.19%	0.55%
Coolant	2.59%	0.00%

Table 20. Comparison of fractional absorption in core components at EOL

System	PB-AHTR	DB-HTR
Fuel	81.77%	96.28%
Coatings	1.36%	0.81%
Matrix	1.58%	0.96%
Pebble shell/blocks	1.41%	1.77%
Coolant	13.88%	0.00%

Figure 22 compares the spectrum at BOL and EOL in the PB-AHTR. The spectrum in a pebble strongly depends on the composition of the neighbor pebbles, and the spectral changes between BOL and EOL are limited – for example at BOL the spectrum shows a deep around 0.3 eV, corresponding to the lowest energy resonance of ^{239}Pu that is highly concentrated in fresh pebbles. On the other hand, the spectrum in the DB-MHR, shown in Figure 23, swings from epithermal at BOL to strongly thermal at EOL.

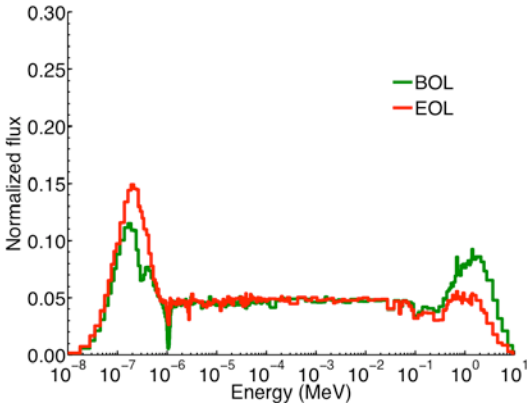

Figure 22. PB-AHTR neutrons spectrum at BOL and EOL

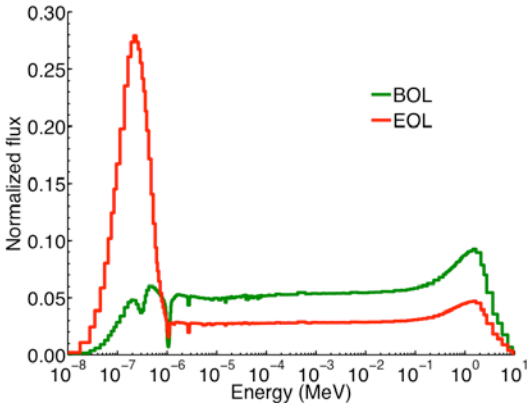

Figure 23. DB-MHR neutrons spectrum at BOL and EOL

The flux changes affect the conversion ratio variations with burnup as shown in Figure 24 – the DB-MHR fuel cycle starts with a hard spectrum and a larger CR (0.37) that increases moderately as fissile isotopes are consumed and the spectrum softens; the PB-AHTR, on the other hand, starts with a softer spectrum and a smaller CR (0.21) that rapidly increases with burnup because the spectrum only slightly changes.

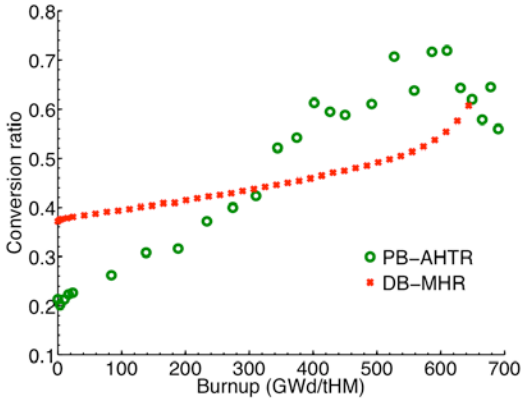

Figure 24 Comparison of the conversion ratio as a function of burnup for the PB-AHTR and the DB-MHR

Table 21 gives the HM composition at EOL and Table 22 compares the consumption of the actinides initially loaded in the reactors. It is noticed that the PB-AHTR consumption of the short-lived ^{241}Pu is slightly smaller although it operates at more than double the power density of the DB-MHR. This is probably due to the spectrum variations illustrated above. Figure 25 shows that the effective fission cross section of ^{241}Pu is almost constant in the PB-AHTR whereas it rapidly increases with burnup in the DB-MHR and towards EOL is about double than in the pebble bed system. The DB-MHR fuel kernels first builds up ^{241}Pu because of its high CR but as the spectrum softens ^{241}Pu burns quickly and its concentration at EOL is smaller than in the PB-AHTR fuel. Figure 26 shows the

^{241}Pu evolution in the two systems. The reduced ^{241}Pu incineration affects the ^{237}Np inventory consumption.

Table 21. Comparison of the heavy metal composition at the EOL in the PB-AHTR and in the DB-MHR fuel.

Nuclide	PB-AHTR	DB-MHR
^{234}U	0.111%	0.230%
^{235}U	0.026%	0.045%
^{236}U	0.008%	0.017%
^{237}Np	6.917%	6.863%
^{238}Np	0.045%	0.053%
^{238}Pu	15.137%	16.095%
^{239}Pu	2.148%	2.165%
^{240}Pu	6.319%	12.271%
^{241}Pu	13.191%	11.834%
^{242}Pu	31.485%	31.486%
^{243}Pu	0.014%	0.008%
^{244}Pu	0.006%	0.003%
^{241}Am	0.488%	0.679%
^{242m}Am	0.009%	0.013%
^{242}Am	0.004%	0.007%
^{243}Am	9.448%	7.155%
^{244}Am	0.016%	0.009%
^{242}Cm	1.715%	1.770%
^{243}Cm	0.079%	0.055%
^{244}Cm	11.687%	8.526%
^{245}Cm	0.957%	0.586%
^{246}Cm	0.187%	0.130%
^{247}Cm	0.003%	0.002%

Table 22. Comparison of feed actinides consumption (%) in the PB-AHTR and in the DB-MHR.

Nuclide	PB-AHTR	DB-HTR
^{237}Np	-65.77	-62.85
^{238}Pu	75.63	104.28
^{239}Pu	-98.54	-98.39
^{240}Pu	-90.76	-80.36
^{241}Pu	-49.56	-50.50
^{242}Pu	116.20	136.52
^{241}Am	-94.13	-91.07
^{242m}Am	-85.47	-75.75
^{243}Am	127.08	88.11

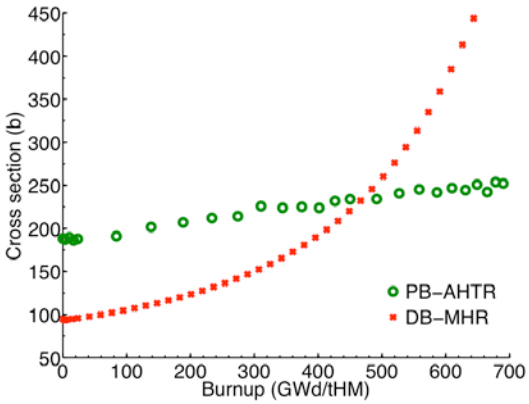

Figure 25. Comparison of the ^{241}Pu effective fission cross section as a function of burnup for the PB-AHTR and the DB-MHR.

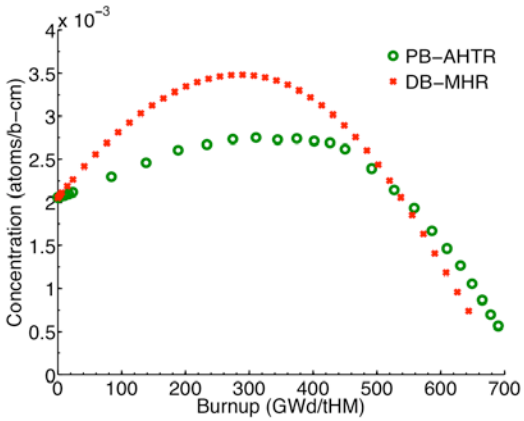

Figure 26. Comparison of ^{241}Pu concentration in fuel kernels as a function of burnup in the PB-AHTR and the DB-MHR.

Tables 23 and 24 compare the fractional neutron absorption in the fuel isotopes at, respectively, BOL and EOL whereas Tables 25 and 26 compare the corresponding contribution of different fuel isotopes to the fission probability.

Table 23 Comparison of fractional absorption in HM at BOL

Nuclide	PB-AHTR	DB-MHR
^{237}Np	2.92%	2.72%
^{238}Pu	0.74%	0.67%
^{239}Pu	56.23%	58.28%
^{240}Pu	25.58%	24.45%
^{241}Pu	8.07%	7.87%
^{242}Pu	2.50%	2.20%
^{241}Am	2.74%	2.73%
^{242m}Am	0.07%	0.07%
^{243}Am	1.15%	1.01%

Table 24. Comparison of fractional fission per actinide at BOL

Nuclide	PB-AHTR	DB-HTR
^{237}Np	0.028%	0.029%
^{238}Pu	0.108%	0.096%
^{239}Pu	84.506%	85.410%
^{240}Pu	0.130%	0.132%
^{241}Pu	15.003%	14.114%
^{242}Pu	0.017%	0.018%
^{241}Am	0.050%	0.049%
^{242m}Am	0.152%	0.147%
^{243}Am	0.007%	0.007%

Table 25. Comparison of fractional absorption per actinide at EOL

Nuclide	PB-AHTR	DB-MHR
^{234}U	0.064%	0.047%
^{235}U	0.049%	0.032%
^{236}U	0.002%	0.002%
^{237}Np	4.566%	3.774%
^{238}Np	0.019%	0.009%
^{238}Pu	14.003%	7.364%
^{239}Pu	14.126%	10.881%
^{240}Pu	15.132%	21.582%
^{241}Pu	29.090%	41.873%
^{242}Pu	10.073%	6.473%
^{243}Pu	0.007%	0.003%
^{244}Pu	0.001%	0.000%
^{241}Am	0.998%	2.313%
^{241m}Am	0.095%	0.235%
^{242}Am	0.043%	0.057%
^{243}Am	5.729%	3.105%
^{244}Am	0.081%	0.026%
^{242}Cm	0.292%	0.142%
^{243}Cm	0.154%	0.060%
^{244}Cm	2.674%	1.098%
^{245}Cm	2.769%	0.917%
^{246}Cm	0.026%	0.006%
^{247}Cm	0.005%	0.001%

Table 26. Comparison of fractional fission per actinide at EOL

Nuclide	PB-AHTR	DB-MHR
^{234}U	0.0008%	0.00%
^{235}U	0.1164%	0.09%
^{237}Np	0.0151%	0.02%
^{238}Pu	1.39%	0.88%
^{239}Pu	26.57%	17.83%
^{240}Pu	0.03%	0.04%
^{241}Pu	63.52%	77.23%
^{242}Pu	0.07%	0.06%
^{243}Pu	0.01%	0.01%
^{241}Am	0.02%	0.03%
^{241m}Am	0.24%	0.43%
^{242}Am	0.04%	0.06%
^{243}Am	0.03%	0.02%
^{244}Am	0.19%	0.10%
^{242}Cm	0.07%	0.05%
^{243}Cm	0.39%	0.18%
^{244}Cm	0.17%	0.07%
^{245}Cm	7.10%	2.91%

Table 27 compares the effective one-group capture cross sections of the fuel isotopes at BOL whereas Table 28 compares the corresponding fission cross sections.

Table 27. Comparison of effective one-group capture cross sections [barn]

Nuclide	PB-AHTR	DB-HTR
^{234}U	40.6	36.6
^{235}U	17.5	14.7
^{236}U	15.9	15.1
^{237}Np	64.2	51.1
^{238}Np	13.3	12.5
^{238}Pu	9.7	8.8
^{239}Pu	86.9	68.4
^{240}Pu	67.8	65.7
^{241}Pu	26.2	20.8
^{242}Pu	25.0	22.9
^{243}Pu	16.8	15.5
^{244}Pu	71.0	56.2
^{241}Am	51.7	38.7
^{241m}Am	152.4	135.5
^{242}Am	214.4	188.7
^{243}Am	82.0	68.2
^{244}Am	47.7	47.6
^{242}Cm	22.3	19.5
^{243}Cm	5.3	4.9
^{244}Cm	252.5	235.9
^{245}Cm	225.1	175.1
^{246}Cm	563.1	409.7
^{247}Cm	90.4	87.0

Figures 29 and 30 compare, respectively, the radiotoxicity and the decay-heat associated with the spent fuel of these deep-burn systems per ton of TRU that is initially loaded in the core. As expected, the PB-AHTR and DB-MHR spent fuel properties are similar. The figures also show the radiotoxicity and decay-heat from 1 ton of TRU in LWRs spent fuel that is sent directly to the repository. For the first hundred years the fission products decay is dominant and deep-burn systems' spent fuel has larger radiotoxicity and decay-heat; after that the situation is reversed until 100 thousand years. But after about one million years differences become very small. Therefore the main advantages of the deep-burn operation are the reduction of the ^{237}Np inventory—a major contributor to the long term dose in the vicinity of the repository, and the better resource utilization—about 650 GWd of thermal energy is generated from one ton of otherwise waste.

Table 28. Comparison of effective one-group fission cross sections [barn]

Nuclide	PB-AHTR	DB-HTR
^{234}U	0.2	0.26
^{235}U	74.2	58.4
^{236}U	0.3	0.27
^{237}Np	0.6	0.54
^{238}Np	0.03	0.04
^{238}Pu	13.7	12.8
^{239}Pu	343.5	270.7
^{240}Pu	0.2	0.22
^{241}Pu	0	0
^{242}Pu	0.6	0.62
^{243}Pu	64.0	57.8
^{244}Pu	291.7	233.7
^{241}Am	2.6	2.3
^{241m}Am	252.6	220.7
^{242}Am	0.3	0.30
^{243}Am	225.8	184.23
^{244}Am	0.15	0.19
^{242}Cm	45.3	39.76
^{243}Cm	0.12	0.16
^{244}Cm	1.66	1.6
^{245}Cm	1148.7	897.6
^{246}Cm	314.4	256.9
^{247}Cm	0.23	0.26

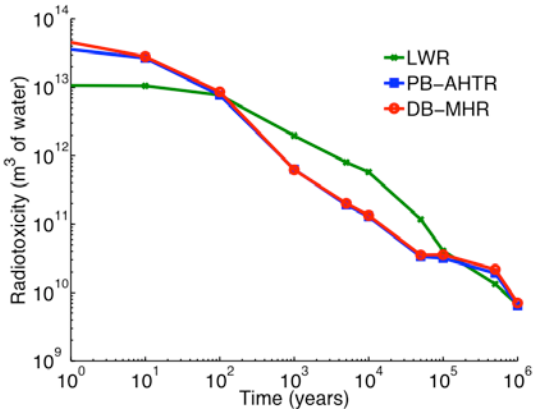

Figure 29 Comparison of spent fuel radiotoxicity per metric ton of initial TRU as a function of decay time after discharge.

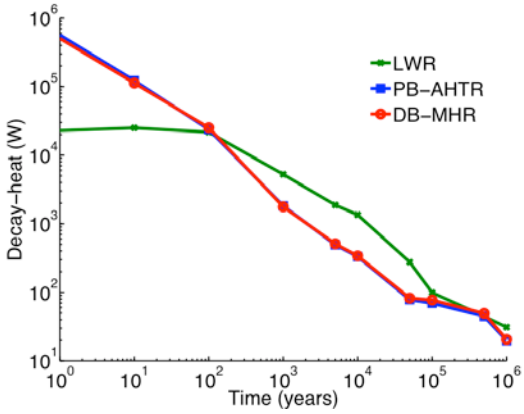

Figure 30. Comparison of spent fuel decay-heat per metric ton of initial TRU as a function of decay time after discharge.

4.4 References

[1] Bardet, P., et al. "The Pebble Recirculation Experiment (PREX) for the AHTR." *GLOBAL 2007*. Boise, Idaho, USA, 2007.

[2] P. Bardet, E. Blandford, M. Fratoni, A. Niquille, E. Greenspan and P. Peterson, "Design, Analysis and Development of the Modular PB-AHTR," Proceedings of ICAPP '08, Anaheim, CA USA, June 8-12, 2008, Paper 8211

[3] M. Fratoni, E. Greenspan and P. Peterson, "Neutronic Design of the Integral and Modular PB-AHTR," International Conference on Reactor Physics, PHYSOR'08, Interlaken, Switzerland, September 14-19, 2008

[4] Venneri, Francesco. "MHR core block design PUMA core specification." General Atomics, 2007.

[5] M. Fratoni, E. Greenspan and P. Peterson, "Neutronic and Depletion Analysis of the PB-AHTR," Proceedings of the Advanced Nuclear Fuel Cycles and Systems, GLOBAL 2007, Boise, ID, September 9-13, 2007

5. Transmutation Capability of the DB-MHR versus that of Hydride Fueled PWR

5.1 Introduction

The University of California at Berkeley recently completed a study of the transmutation ability of hydride fuel in PWR [1-4]. The reference hydride fuel examined is U-PuH_2-$ZrH_{1.6}$ (abbreviated as PUZH). The plutonium transmutation capability of this hydride fuel in PWR was compared against that attainable using MOX fuel.

It was found [1-4] that for plutonium loading that gives the reference PWR cycle length when using the reference PWR core geometry, the PUZH fuel achieves more than double the average discharge burnup than MOX fuel, when both fuels are uniformly distributed throughout the core. That is, the recycling of plutonium in PUZH fuel in the reference PWR geometry offers doubling of the fraction of plutonium transmuted, smaller fissile plutonium fraction in the discharged fuel, reduction of the inventory of minor actinides (MA) generated, a higher decay heat and neutron emission rate per unit mass of Pu or TRU, smaller inventory of ^{237}Np and its precursors, but comparable radiation levels and decay heat per discharged fuel assembly. As a result, the use of PUZH rather than MOX fuel is expected to significantly increase the effective repository capacity. The higher specific neutron yield and decay heat in the discharged TRU is expected to make the spent PUZH fuel more proliferation resistant than the MOX fuel, while the handling of the spent fuel assemblies are expected to require similar precautions as for the MOX fuel. Using thorium hydride instead of zirconium hydride and eliminating the uranium, it is possible to obtain an even better fractional transmutation – incinerating 62.5% of the loaded plutonium. This is likely to be the maximum possible fractional transmutation of plutonium possible to achieve in a single pass through a PWR.

This section compares the transmutation-ability of TRU in TRU hydride fueled PWR with those of the DB-HTR and PB-AHTR. The comparison is done for a single recycle. The TRU composition used for this comparison is that of Table 3. No uranium and no curium are loaded into the fuel.

5.2 TRU transmutation-ability of PWR

Due to the limited information available on the physical properties of the hydrides, the following assumptions were made:

1) The MA form hydrides of the form AmH_2, CmH_2 etc. that are stable at reactor operating conditions;
2) The MA-hydrides have a density equal to that of PuH_2 – 10.4 g/cm^3.

Table 29 compares selected characteristics of TRU recycling in PWR using hydride fuel and in the two TRISO fuel containing core designs being examined – the DB-MHR and the PB-AHTR. A single recycling is assumed. It is found that the attainable burnup from the hydride fueled PWR is significantly smaller than that from the DB-MHR and the PB-AHTR while the specific TRU loading is higher and the fuel residence time is longer. The fraction of TRU fissioned per pass through the core is 46% in the PWR versus 64% in the DB-MHR and 66.5% in the PB-AHTR. The corresponding values for the fraction of plutonium incinerated are 50%, 74% and 70%. The PWR discharged plutonium also

has a higher fissile fuel content, a smaller minor actinides fraction and, correspondingly, a lower specific decay heat and neutron emission rate.

Table 29 Comparison of selected characteristics of TRU recycling in PWR using hydride fuel and in two TRISO fuel containing core designs; single recycling

Property	DB-MHR	PB-AHTR	TRU hydride
Thermal Power (MW_{th})	600	2400	3280
Initial Pu loading (kg/MW_{th})	1.517	0.704	2.790
Initial Np loading (kg/MW_{th})	0.117	0.054	0.213
Initial Am loading (kg/MW_{th})	0.067	0.033	0.131
Initial Cm loading (kg/MW_{th})	0	0	0
Attainable burnup (GWD/MtiHM)	621.3	653.5	456.1
Fuel residence time (EFPD)	1052	518	1430.3
At discharge			
Total TRU inventory ($kg/GWD/_{th}$)	0.579	0.514	1.187
% TRU incinerated/cycle	64.0%	66.5%	45.8%
Pu inventory (kg/GWD_{th})	0.429	0.351	0.981
% Pu incinerated/cycle	70.1%	74.3%	49.8%
Pu inventory/ initial Pu	29.9%	25.8%	50.2%
^{238}Pu	200.2%	175.4%	205.0%
^{239}Pu	1.6%	1.5%	14.2%
^{240}Pu	19.2%	9.2%	63.4%
^{241}Pu	48.5%	50.4%	104.6%
^{242}Pu	231.8%	215.9%	160.7%
Fissile Pu/ Tot Pu	18.9%	22.4%	36.4%
U inventory (kg/GWD_{th})	1.70E-3	7.46E-4	3.09E-3
^{234}U	1.33E-3	5.71E-4	2.35E-3
^{235}U	2.62E-4	1.34E-4	5.49E-4
^{236}U	9.94E-5	4.11E-5	1.93E-4
MA inventory (kg/GWD_{th})	0.150	0.162	0.207
Np	0.040	0.036	0.070
Am	0.046	0.051	0.082
Cm	0.064	0.075	0.054
$^{237}Np+^{241}Am+^{245}Cm$	0.047	0.043	0.103
MA/Pu at discharge	0.35	0.46	0.21
Neutron source (n/s/gHM)	1.180E6	1.483E6	4.786E5
Activity (Ci/gHM)	288.78	446.91	97.67
Decay heat (W/gHM)	2.71	2.91	1.17
Gamma decay heat (W/gHM)	0.032	0.055	0.008
Neutrons per g Pu (n/s)	1662.8	1655.8	1112.3
Specific heat (w/g Pu)	0.450	0.741	0.147

Figures 31 and 32 show that the neutron spectrum in the PuH_2-$ZrH_{1.6}$ fuel significantly differs from the spectra in the DB-MHR and PB-AHTR fuel. It may be that the attainable

burnup could be increased by increasing the water-to-fuel volume ratio of the PWR. Table 30 compares the fractional neutron absorption in the different fuel isotopes at BOL.

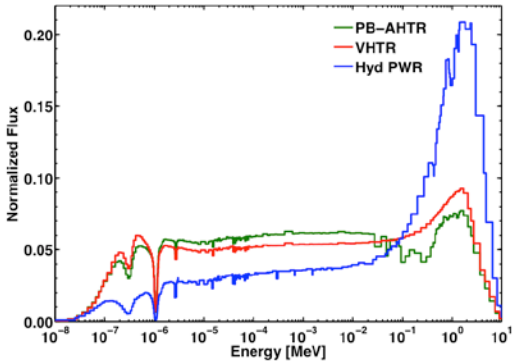

Figure 31 Comparison of the BOL neutron spectrum in the fuel of hydride fueled PWR, DB-MHR and PB-AHTR

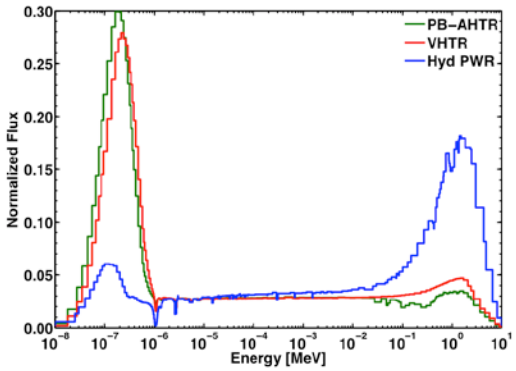

Figure 32 Comparison of EOL neutron spectrum in the fuel of hydride fueled PWR, DB-MHR and PB-AHTR

Table 30 Comparison of fractional absorption in HM at BOL

Nuclide	PB-AHTR	DB-MHR	TRU hydride
^{237}Np	2.92%	2.72%	3.64%
^{238}Pu	0.74%	0.67%	0.87%
^{239}Pu	56.23%	58.28%	57.27%
^{240}Pu	25.58%	24.45%	20.45%
^{241}Pu	8.07%	7.87%	10.97%
^{242}Pu	2.50%	2.20%	2.29%
^{241}Am	2.74%	2.73%	3.09%
^{242m}Am	0.07%	0.07%	0.10%
^{243}Am	1.15%	1.01%	1.31%

5. 3 References

[1] F. Ganda and E. Greenspan, "Incineration of Plutonium in PWR Using Hydride Fuel," Proc. 2005 International Conference on Advances in Nuclear Power Plants; ICAPP–2005, Seoul, Korea, May 15-19, 2005.

[2] F. Ganda and E. Greenspan, "Plutonium Incineration Capability of Hydride Versus MOX Fuel in PWR" Proceedings of GLOBAL'05, Tsukuba, Japan, October 9-13, 2005.

[3] F. Ganda and E. Greenspan, "Reactor Physics of Hydride Fueled PWR Cores" Advances in Nuclear Analysis and Simulation, PHYSOR 2006, Vancouver, BC, Canada, September 10 - 14, 2006.

[4] F. Ganda and E. Greenspan, "Plutonium recycling in hydride fueled PWR cores," Submitted to Nuclear Engineering and Design, May 2008

6. Conclusions

It has been confirmed that the TRU from fuel discharged from LWR at 50,000 GWd/tHM that is loaded into a deep-burn modular high-temperature reactor (DB-MHR) design developed by General Atomics after 10 years of cooling can undergo, in a single pass through the core, a burnup exceeding 60%. The maximum attainable burnup achieved in our analysis is 620 GWd/tTRU corresponding to the consumption/destruction of 63% of the loaded TRU, of nearly 70% of the loaded plutonium and of 91% of the loaded fissile plutonium. The inventory of long-lived ^{237}Np and its precursors (^{241}Pu, ^{241}Np, ^{245}Cm, ^{249}Bk) are reduced by ~58% and their transmutation is particularly sensitive to C/HM because softer spectra can better fission ^{241}Pu.

The burnup attainable using a large liquid salt rather than helium for the coolant and pebble rather than prismatic fuel is 650 GWd/tTRU. The corresponding consumption/destruction of the loaded fuel is 66.4% of the TRU, 74% of the plutonium,

91% of the fissile plutonium and 58% of the ^{237}Np and its precursors. The optimal C/HM ratio for the two reactor systems is ~2,500.

For comparison, the best transmutation characteristics of TRU in PWR are inferior if limited to a single pass through the core – the discharge burnup is 456 GWd/tTRU corresponding to the destruction of 46% of the loaded TRU and nearly 50% of the loaded Pu. The specific TRU and Pu loading in the PWR are approximately twice that in the TRISO fueled cores while the specific decay heat and specific spontaneous neutron yield of the PWR discharged fuel are significantly smaller. The specific inventory of ^{237}Np and its precursors in the fuel discharged from the PWR is approximately twice that of the TRISO fueled cores. The neutron spectrum of the PWR studied is significantly harder than the spectrum of the TRISO-fueled cores. By optimizing designing the spectrum of the TRU loaded PWR core it may be possible to improve its transmutation ability.

It is concluded that the TRU transmutation ability of the DB-MHR are, indeed, superior to those of PWRs. Relative to the DB-MHR, the PB-AHTR offers nearly 5% higher fractional reduction in the inventory of TRU and plutonium while requiring only half of the specific TRU loading. These performance benefits are due to the use of liquid-salt instead of helium coolant that enables operating the PB-AHTR at a higher power density and higher specific power, and to the use of pebbles rather than prismatic fuel that enable continuous refueling. It would be interesting to add to the above comparison helium-cooled pebble-bed reactor and liquid-salt cooled prismatic fuel reactor.